Contents lists available at [ScienceDirect](https://www.sciencedirect.com)

## International Journal of Disaster Risk Reduction

journal homepage: [www.elsevier.com/locate/ijdr](http://www.elsevier.com/locate/ijdr)

# Hail hazard modeling with uncertainty analysis and roof damage estimation of residential buildings in North America

Yao Li <sup>a</sup>, Keith Porter <sup>b</sup>, Katsuichiro Goda <sup>a, c, \*</sup><sup>a</sup> Department of Statistical and Actuarial Sciences, London, Ontario, Canada<sup>b</sup> Institute for Catastrophic Loss Reduction, Canada<sup>c</sup> Department of Earth Sciences, London, Ontario, Canada

## ARTICLE INFO

## Keywords:

Hail hazard  
Roof damage  
Model uncertainty  
Monte Carlo simulation

## ABSTRACT

This research presents a statistical approach for hail risk modeling that incorporates the uncertainties of hail model prediction to provide insight into assessing the roof damage of a residential house in hail events. By quantifying the inherent uncertainties in evaluating hailstorm characteristics, this study extends the current existing hail models. The hail data are sourced from the Community Collaborative Rain, Hail and Snow Network (CoCoRaHS) in the U.S. In the modeling process, the largest hail diameter reported in the CoCoRaHS database serves as a primary input variable to estimate the number of observations for the largest hail diameter, hailstorm duration, and hit rate. The assessment of hail risk in this study focuses on the probability of hail damage and resultant repair costs for five types of roofs in North America (unrated roof and impact-resistant roofs with UL 2218 rating classes 1 to 4). The probability of hail damage is calculated as the failure probability by integrating all individual hailstone hits having variable diameters during a hailstorm with fragility curves, which estimate the probability that hailstones will fracture asphalt shingles (allowing water infiltration) or that they dislodge enough granules to cause visible damage requiring replacement for aesthetic reasons. The results reveal that an impact-resistant roof (impact-resistant rating classes 1 to 4) is associated with lower hail risks, with 60 % to 98 % reduction on average compared to unrated roofs. This study provides a comprehensive uncertainty modeling approach for hail hazard and risk, enabling better-informed decision-making and risk management strategies.

## 1. Introduction

Hailstones are pieces of ice that fall from convective hailstorms. Hail forms when vapor or rain rises into freezing air, carried by a strong updraft typically seen in summer [1]. Hailstones increase in size as they encounter liquid water droplets that freeze upon contacting the surface of the hailstone. The intensity of the updraft influences the length of time the hail stays in the freezing air. Longer time leads to larger hailstones, though as the hailstone falls through the warm air mass closer to the ground, melting reduces its size. The hailstone falls when the thunderstorm's updraft is no longer able to uphold the weight of the hailstone. Hailstones vary in size, ranging from a defined minimum size of 5 mm diameter (below which frozen hydrometeors are called graupel [2]) to over 200 mm [3]. For the purposes of this study, hailstones are defined as ice descending from thunderstorms with 5 mm or larger diameters.

Hailstorms cause significant impact on a global scale. They damage buildings, vehicles, crops, and injure livestock and people. Hailstorms can be so costly that they affect regional economies [4–9]. In 2013, Germany experienced a € 3.6 billion loss due to hail

\* Corresponding author. Department of Statistical and Actuarial Sciences, London, Ontario, Canada.

E-mail address: [kgoda2@uwo.ca](mailto:kgoda2@uwo.ca) (K. Goda).

<https://doi.org/10.1016/j.ijdr.2024.104853>

Received 6 August 2024; Received in revised form 20 September 2024; Accepted 20 September 2024

Available online 23 September 2024

2212-4209/© 2024 The Authors. Published by Elsevier Ltd. This is an open access article under the CC BY license (<http://creativecommons.org/licenses/by/4.0/>).

[10]. In North America, a US\$ 2.3 billion loss in Denver, Colorado, U.S., in 2017 [11], and over CAD\$ 1.2 billion in losses caused by hail in Calgary, Alberta, Canada, in 2020 [12]. In light of losses like these, meteorologists and engineers have sought to better understand hailstorms, to develop warning systems, to develop hail-resistant building materials, and to improve methods to test and demonstrate the efficacy of those materials.

Understanding past hailstorms can help us estimate what will happen in the future. Existing methodologies for assessing hail hazard encompass several approaches including kinetic energy [13–16], radar reflection from the air [16–19], satellite detection [20,21], and the largest hail diameter on the ground-level from hailpads [22,23]. Each approach has advantages and disadvantages. Kinetic energy calculations provide insights into the damage potential, considering mass and velocity, but the kinetic energy of a particle is only partly indicative of its damage potential, for several reasons. Hailstones have irregular shapes with protrusions that can concentrate pressure. Some of a hailstone's kinetic energy gets absorbed by fracturing the hailstone. The duration of impact affects the peak force that the hailstone imparts on a shingle. Radar reflection and satellite detection enable large-scale, real-time or near-real-time monitoring, though they only provide indirect size estimates that can be influenced by environmental factors and are limited by calibration and resolution. Estimating hail risk through diameter offers direct, relatable measures but faces challenges in accurate sampling and variability in hailstone shapes. The hailpad approach provides tangible evidence of hailstone size on ground, capturing the imprints of hailstones to measure their size distribution directly. The challenge of hailpads lies in the effort of securing locations and traveling across large areas to manage them.

To model hail risk, hail size distribution and fragility to properties are crucial elements. Various relationships for the hailstone size distribution have been developed by Ref. [22] using data from the Community Collaborative Rain, Hail, and Snow Network (CoCoRaHS; <https://www.cocorahs.org/>) in the U.S. CoCoRaHS is a network that provides the average and largest hail diameters, duration, and number of hailstones for fitting the hailstone size relationship (distribution), duration relationship, and hit rate relationship [22]. In Ref. [24], the largest hail diameter was used as the key input to the relationships of the size distribution, hit rate, and duration from Ref. [22], and fragility curves for five types of roofs (unrated roof and impact-resistant roofs with rating classes 1 to 4) were developed to relate the maximum diameter to the probability of hail damage at the scale of individual shingles and of the entire roof [22]. offered probabilistic relationships between maximum diameter, hit rate, and duration, but [24] only propagated some of the hailstone size and count uncertainties through the loss model.

This study uses CoCoRaHS data to develop a statistical model that derives the predictive equations of the largest hail diameter, duration, and hit rate of a hailstorm and estimate the risk in terms of the probability of hail damage on residential house roofs by considering the uncertainty. This study utilizes the methodology of [22] as a foundation for calibrating hail relationships, specifically characterizing the distribution of the largest hail diameter given a hailstorm (via an exponential function), the duration of hailstorms (using a power function), and the hit rate (using a power function) as functions of the largest hail diameter. This study evaluates the potential hail damage in terms of the probability of hail roof damage applying the fragility curve model presented by Ref. [24]. The novelty of this research consists of: (i) new data filtration process to explore more CoCoRaHS data, (ii) more comprehensive uncertainty statistical relationship for hail hazards, and (iii) evaluating the probability of hail damage on roofs utilizing the hail model that propagates more uncertainties.

## 2. CoCoRaHS data and hail relationships

The hail observation data used in this study are from CoCoRaHS in the U.S. CoCoRaHS is a volunteered network that uses hailpads to collect the hail information. It features a hailpad, a 12-inch square (0.0929 m<sup>2</sup>) surface used for recording dents left by hailstones. Volunteers need to fill in a hail report (Fig. 1) to record the data derived from the hailpad. Key variables derived from the hailpad include the largest hail diameter, which refers to the size of the biggest hailstone recorded, and the average hail diameter, which calculates the mean size of all collected hailstones. Additionally, the total number of hailstones and the duration of the hail event are recorded. These variables are crucial for various components of a hail hazard model (Fig. 2).

The CoCoRaHS network started its operation in 1998 and has gathered 46,138 observations by February 2023 (Fig. 3a). This represents an increase of over 8000 hail cases from the counts reported by Ref. [22], prior to data screening. This study implements the data screening procedure as adopted by Ref. [22] by: (1) excluding cases that have missing values among the five relevant columns, (2) excluding cases with an uncertainty duration over 3 minutes, (3) excluding observations with duration over 40 min, and (4) excluding cases with fewer than five hailstones on a hailpad. The reason behind each data screening criterion can be found in Ref. [22]. The present study adopted two new filters: (1) equal-diameter cases, which requires that the largest diameter equals or exceeds the average diameter, and (2) the average diameter must equal or exceed the smallest during a hailstorm. This is different from Ref. [22], who required that the largest diameter be strictly greater than the average diameter and that the average needs to be strictly greater than the smallest diameter. To replicate the findings of [22] and to investigate the extended dataset, this study first reproduced their result using data (1413 observations) by their screening rules (for a comparison purpose, see Appendix Figure A1 and Table A1), and then encompasses the complete dataset (3413 observations) for the main result. The success in replicating prior research findings confirmed that this approach was implemented correctly, and an expansion of the dataset enhances the statistical power and realistic feature of the hailstorm, providing a more robust basis for drawing conclusions and making decisions.

After data screening, the dataset contains 3413 cases (more than doubled the previous cleaned data size of 1413). Fig. 3b illustrates the 3413 hail events, representing 7.4 % of the original data retained for analysis. It is posited that the average diameter, duration, and hit rate correlate with the diameter of the largest hailstone. The average diameter is instrumental in estimating the Gamma parameter for the hailstone size distribution within a hailstorm. The total count of hailstones in a single event divided by the duration gives the hit rate. By simulating the number and distribution of hailstones in an event based on the largest diameter, it is possible to

## CoCoRaHS HAIL REPORT

www.cocorahs.org

Station Number: \_\_\_\_\_  
 Station Name: \_\_\_\_\_

Name: \_\_\_\_\_ Phone: \_\_\_\_\_

Home Address: \_\_\_\_\_

Location of Hail (if different from Home): \_\_\_\_\_

Date of Storm: \_\_\_\_\_ Time Hail Began: \_\_\_\_\_ am / pm Hail Lasted: \_\_\_\_\_ minutes

Your time of hail beginning is correct within:  1 min.  2 min.  3-5 min.  10 or more minutes

Stone Size (inches)	Rice 1/8"	Pea 1/4"	3/8"	1/2"	Grape 3/4"	Penny 3/4"	Quarter 1"	Hail Diner 1 1/4"	Popcorn 1 1/2"	Golfball 1 3/4"	Fast Egg 2"	Tennis 2 1/2"	Teslap 3"	Grapfruit 4"	Softball 4 1/2"	Other (give diameter)
Largest	<input type="checkbox"/>	_____														
Smallest	<input type="checkbox"/>	_____														
Most Common	<input type="checkbox"/>	_____														

Check All That Apply:

Hailfall was:  continuous  intermittent → Was there more rain than hail?  Yes  No

Hailstones were:  hard  soft  mixed → Color of Hail was:  white ice  clear ice

Hail started:  before rain  after rain  at same time as rain → Was Hail Preserved?  Yes  No

Largest hail started:  before smaller hail  after smaller hail  at same time as smaller hail

Damage:  none  minor leaf damage  dents in cars  broken house windows  crop damage  
 (Check all that apply)  shredded leaves  damaged roofs/shingles  broken car windows  (other) \_\_\_\_\_

Hail Pad Average distance between hailstones \_\_\_\_\_ inches OR depth of hail on ground \_\_\_\_\_ inches  
 Information: OR Number of indentations on your hailpad \_\_\_\_\_

Remarks: \_\_\_\_\_

Fig. 1. CoCoRaHS hail report sheet. The hailstone size is a categorical variable in this sheet. The hailstone size bin width is different depending on thresholds, 1/8 inches between 0 and 1 inch, 1/4 inches between 1 and 2 inches, and 1/2 inches between 2 and 3 inches. Detailed hailpad information can be found in <https://www.cocorahs.org/Content.aspx?page=HailPadDropOff>.

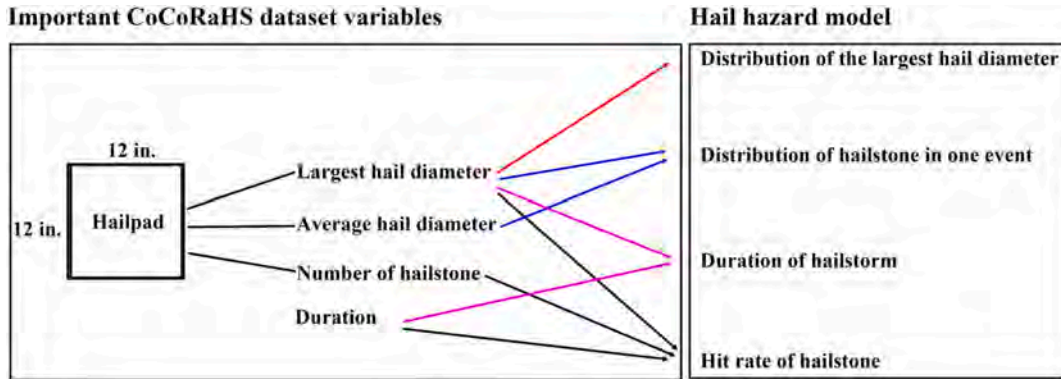


Fig. 2. CoCoRaHS variables associated with a hail hazard model. The distribution of the largest hail diameter is fitted using the observed largest hail diameters. The distribution of hailstones in a hailstorm is fitted by both largest hail and average hail diameters. The duration statistical relationship is fitted by the largest hail diameter and duration. The hit rate statistical relationship is fitted by the largest hail diameter, duration, and number of hailstones.

assess the probability of each hailstone causing roof damage using fragility curves by Ref. [24] (details will be mentioned in Section 3).

The following four subsections present the details of characterizing (1) the diameter of the largest hailstone  $D_l$ , (2) the relationship between  $D_l$  and diameter of the average hailstone, (3) the relationship between  $D_l$  and hailstorm duration, and (4) the relationship between  $D_l$  and hit rate.

### 2.1. Diameter of the largest hailstone

The largest hailstone diameter pertains to the greatest hail dent diameter observed on a single hailpad. The majority of hailpads captured hailstones with diameters smaller than 1 inch (Fig. 4a), with only two largest instances of hailstones measuring 2.75 inches documented from 2005 to 2010 (Fig. 4b). The maximum diameter of the largest hailstones generally coincided with years that exhibited a higher frequency of observations. Between 1998 and 2023, the central region experienced a significant increase in both the number of hail events and the maximum diameters recorded by hailpads. However, the potential impacts of climate change over years are not factored into this study.

Hailstones often deviate from a perfect spherical shape and can generally be grouped into three categories: conical, spheroidal, and irregular [25–27]. To be consistent with the relationship by Ref. [22] for the number of observations, a perfect spherical shape of a hailstone is required, and the diameter needs to be converted from the original gathered diameter data, which is in inches, to millimeters (1 inch = 25.4 mm). To convert the irregular shape of a hailstone to a perfect spherical ice ball, the ice's mass ( $m$ ) is first estimated by its maximum diameter ( $D_{max}$  in cm) using the following equation [28]

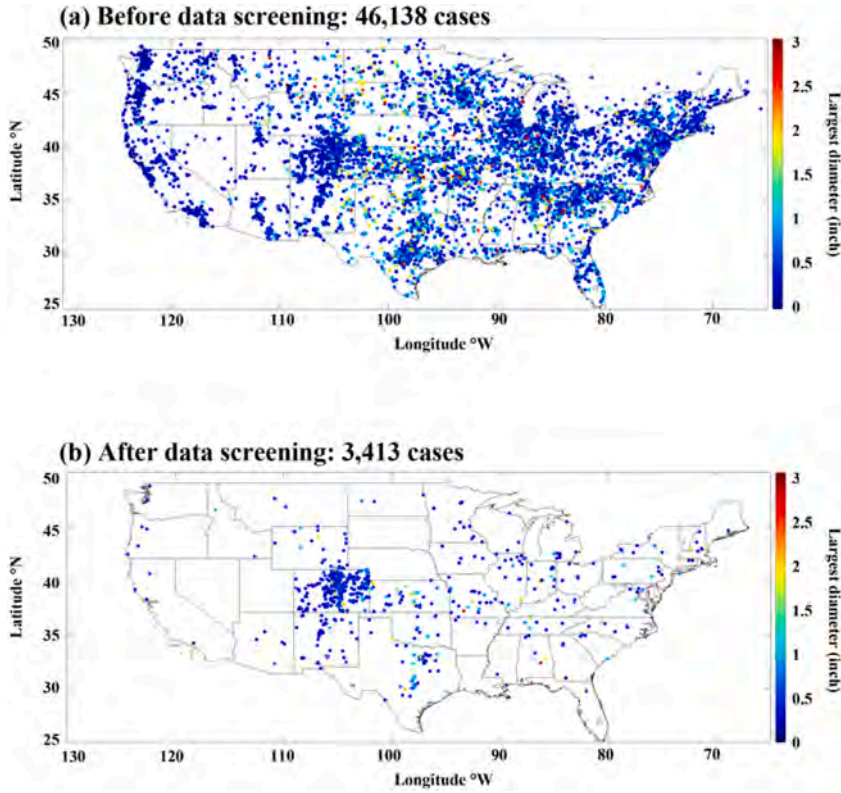


Fig. 3. Maps of hail cases. The original dataset contains total of 46,138 cases of hail observations whose information is collected by CoCoRaHS from May 1998 to February 2023. After data screening, 3413 cases were retained for analysis. The dot positions indicate the locations of the hailpads. The color of the dot represents how large the largest diameter is collected on the hailpad. The largest hail diameter is 2.75 inches in the data for analysis.

$$m = 0.372D_{max}^{2.69}. \tag{1}$$

The volume equation of a sphere is given by

$$V = \frac{4}{3}\pi\left(\frac{D_e}{2}\right)^3, \tag{2}$$

where  $D_e$  is the equivalent diameter of a perfect sphere. By solving the following equation

$$\rho V = m, \tag{3}$$

where  $\rho$  is the density of hail, which is set to 0.91 g/cm<sup>3</sup> in this study [22],  $D_e$  (in cm) is calculated as

$$D_e = \left(\frac{6(0.372D_{max}^{2.69})}{\pi\rho}\right)^{\frac{1}{3}}. \tag{4}$$

Finally, the calculated value of  $D_e$  is converted to mm and denoted by  $D_l$ . In the reporting format used by CoCoRaHS, the largest hailstone diameters are classified into categories, such as rice-sized (0.125 inches), grape-sized (0.625 inches), tennis ball-sized (2.5 inches), among others. Each category is associated with a specific numerical value in inches that quantifies the size of the hailstone (Fig. 1). The dataset includes thirteen distinct values that serve to quantify the size of the hailstone diameters. Table 1 shows the thirteen unique values of the largest hail diameter in different units and their transformed diameters for a perfect sphere.

The  $D_l$  range is from 6.1 to 52.6 mm. The data points in Fig. 4c show the empirical relationship between  $D_l$  and the corresponding number of observational records. To capture the essence of this relationship, an exponential function (representing as a natural-log form in Equation (5)) is employed to model the observed decrease in the number of hail observations.

$$\log(nObs(x)) = m_{DL}x + b_{DL} + \epsilon_{DL}. \tag{5}$$

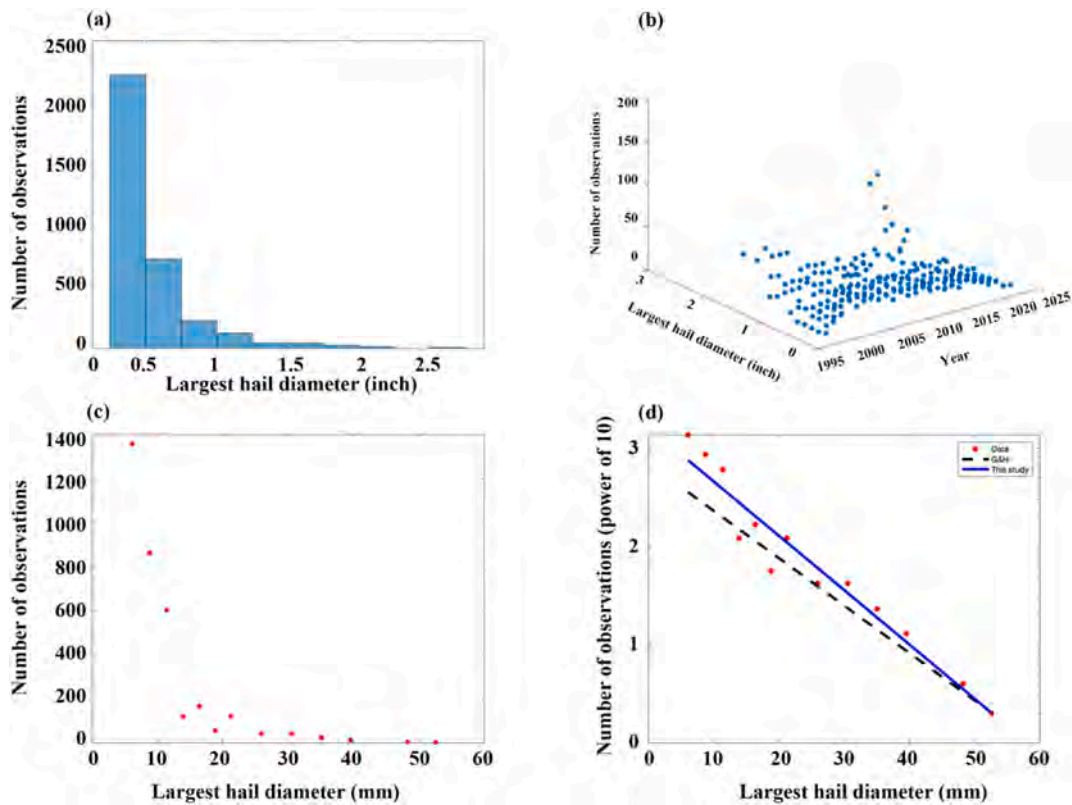


Fig. 4. Largest hail diameter plots. (a) Histogram of largest hail diameter. (b) 3D scatter plot of the number of observations of the largest hailstone diameter over years. (c) Number of observations on each  $D_l$ . (d)  $D_l$  relationship comparison plot. G&H represents the function fitted in previous study [22].

Table 1  
Unique largest hail diameters in different units and shapes.

Category of the largest hail diameter	Original largest hail diameter (inch)	Original largest hail diameter (mm)	Perfect sphere hail diameter $D_l$ (mm)
1	0.250	6.4	6.1
2	0.375	9.5	8.8
3	0.500	12.7	11.4
4	0.625	15.9	13.9
5	0.750	19.1	16.4
6	0.875	22.2	18.8
7	1.000	25.4	21.2
8	1.250	31.8	25.9
9	1.500	38.1	30.6
10	1.750	44.5	35.1
11	2.000	50.8	39.5
12	2.500	63.5	48.3
13	2.750	69.9	52.6

where  $m_{DL} = -0.1273$ , with 95 % confidence interval  $(-0.1485, -0.106)$ ,  $b_{DL} = 7.4$ , with 95 % confidence interval  $(6.781, 8.019)$ , and an error term  $\epsilon_{DL} \sim Normal(0, 0.21)$  with  $p$ -value of 0.927 in Kolmogorov-Smirnov test (note:  $Normal(\mu, \sigma^2)$  represents the normal distribution with mean  $\mu$  and variance  $\sigma^2$ ). Fig. 4d shows that the  $D_l$  distribution has an exponential decreasing trend similar to Ref. [22]. The black and blue lines represent the statistical relationship fitted by Ref. [22] and this study, respectively. This statistical relationship reflects how the frequency of hail observations changes as  $D_l$  grows, which is consistent with meteorological observations and theoretical expectations [22,29,30]. Fig. 5 shows the uncertainty in the  $D_l$  sample size statistical relationship. The dark grey area in Fig. 5 represents the 95 % confidence interval around the best-fit line, suggesting the range in which the true mean number of observations is expected to fall. The light grey area in Fig. 5 corresponds to the 95 % prediction interval, providing an estimate of where the future data points are likely to lie. The presence of uncertainty in the number of observations for  $D_l$  is a critical factor that should be considered in the  $D_l$  distribution. Details about the uncertainty analysis on the distribution of  $D_l$  will be mentioned in Section 3.

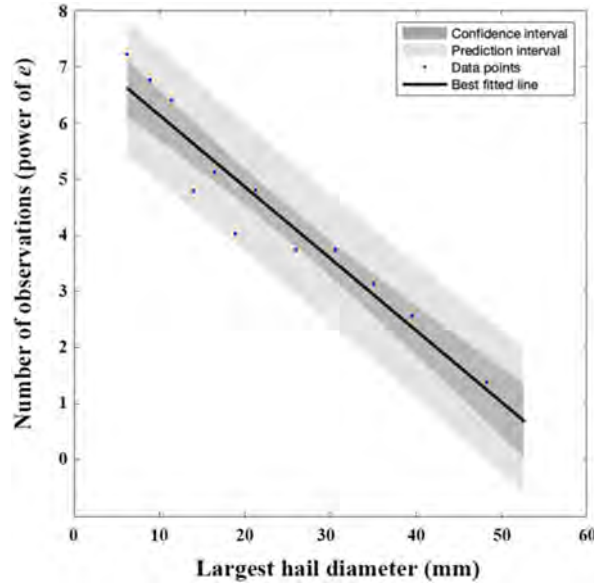


Fig. 5. Log-based  $D_l$  sample size statistical relationship. The plot displays the number of observations under each  $D_l$  as the blue data points and a best fitted line as an exponential function (Equation (5)). The dark grey area represents the 95 % confidence interval for the true mean number of observations for the largest hail diameter. The light grey area represents the 95 % prediction interval.

2.2. RELATIONSHIP BETWEEN  $D_l$  AND  $D_a$

The diameter of hailstones aloft during a hailstorm follows an exponential distribution [31], while the diameter of hailstones on ground follows a Gamma distribution [31–34]. In the on-ground hailstone simulation process of this study,  $D_l$  is first simulated. Then, given  $D_b$ , the hailstone diameter ( $D$ ) in a hypothetical hailstorm is simulated in the range from 5 mm to  $D_l$ . The traditional Gamma distribution spans from 0 to infinity, which may generate  $D$  that is greater than  $D_b$ , conflicting with the first condition of the simulation process. Therefore, a renormalized Gamma distribution is applied here to represent the probability distribution of hailstone diameters that fall between 5 mm and  $D_l$ . The cumulative distribution function of the hailstone diameter ( $F_D(d)$ ) is given by

$$F_D(d) = \frac{\int_5^d \frac{\beta^\alpha x^{\alpha-1} \exp(-\beta x)}{\Gamma(\alpha)} dx}{\int_5^{D_l} \frac{\beta^\alpha x^{\alpha-1} \exp(-\beta x)}{\Gamma(\alpha)} dx} \tag{6}$$

The parameters  $\alpha$  (shape parameter) and  $\beta$  (inverse scale parameter) in the Gamma distribution have a relationship with the mean of hail diameter distribution ( $\mu_d$ )

$$\beta = \frac{\alpha}{\mu_d} \tag{7}$$

This study assumes that the mean of the Gamma distribution can be substituted by the average hail diameter of a perfect sphere denoted by  $D_a$ . To estimate the parameters of the Gamma distribution, an approximate value of  $\alpha$  is taken from Ref. [32], in which the Gamma distribution was used to characterize the size distribution of hail data in Alberta. Then,  $\beta$  can be calculated by Equation (7). A key limitation of this approach is the arbitrary selection of  $\alpha$  values, as there is no established reference to guide these choices for hailpad. Ref. [32] has provided guidance on selecting the shape factor for real hailstone on ground. The longer the time after the hailstones have hit the ground, the smaller the shape factor becomes due to ground-level melting [32]. Note that the situations in this study and [32] are different. The hailpad dents in this study are minimally affected by ground-level melting, which contrasts with the factors considered in Ref. [32]. To consider the uncertainty associated with  $\alpha$ , three values of  $\alpha = 1.5, 1.75,$  and  $2.0$  are used in the later section of the paper.  $F_D(d)$ , adjusting the area under the probability density function between 5 mm and  $D_l$  to one, is used in Section 3 for Monte Carlo simulations.  $D_a$  can be estimated by a power function of  $D_l$  (see Fig. 6) [22]

$$\log_{10}(D_a) = \log_{10}(a_{D_a}) + b_{D_a} \log_{10}(D_l) + \epsilon_{D_a} \tag{8}$$

where  $a_{D_a} = 1.122$ , with 95 % confidence interval (0.815, 1.543),  $b_{D_a} = 0.7511$ , with 95 % confidence interval (0.6487, 0.8535), and an error term  $\epsilon_{D_a} \sim Normal(0, 0.018)$ . In this study, Fig. 6d shows that the  $D_a$  relationship is similar to Ref. [22]. The black and blue lines represent the statistical relationship fitted by Ref. [22] and this study, respectively.

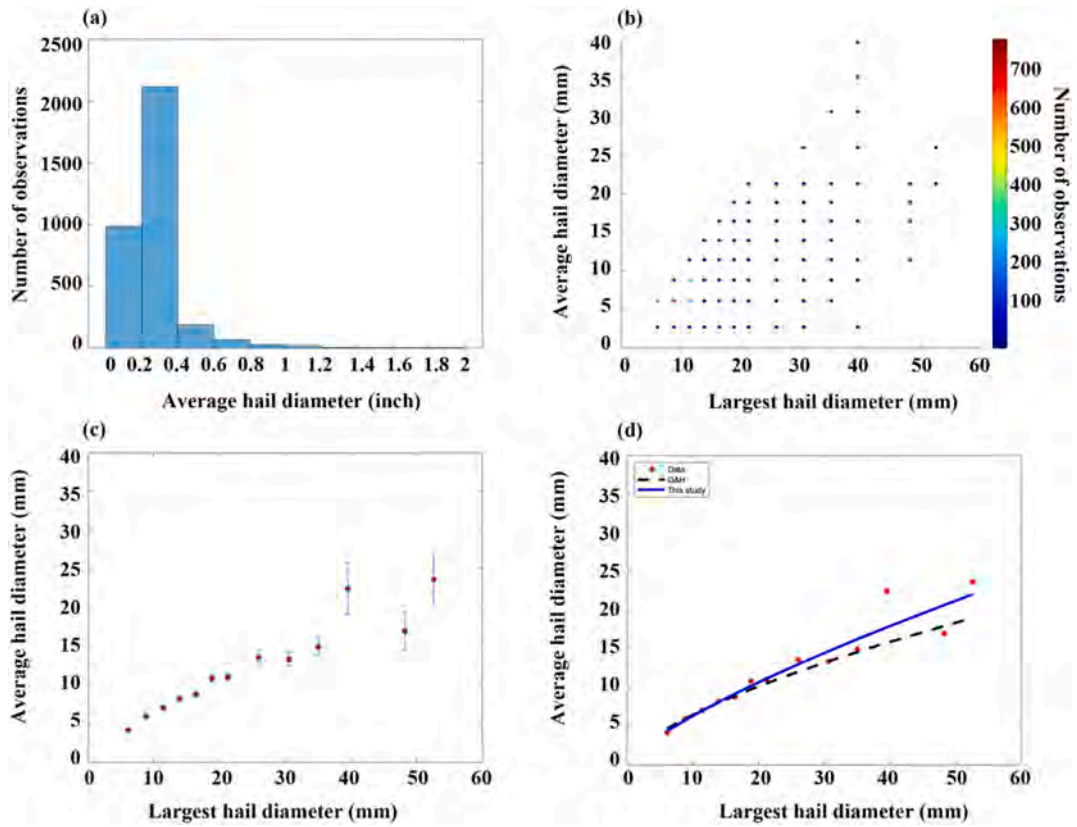


Fig. 6. Average hail diameter plots. (a) Histogram of average hail diameter. (b) The scatter plot of  $D_a$  under each unique  $D_l$ , with color indicating the number of observations. (c) Averaged  $D_a$  plot with variation bar. The wider bar indicates that the variance is large due to a smaller number of observations and a high degree of variation in individual values. (d)  $D_a$  statistical relationship comparison plot.

Fig. 7 highlights significant uncertainty in predicting the average hail diameter based on the largest hailstones, as evidenced by the wide prediction interval. As  $D_l$  increases, the interval range expands, which corresponds to wider variation bars in Fig. 6c. The variability in predicting the average hail diameter poses a challenge for accurate forecasting  $F_D(d)$ , which influences the simulation for the number of hailstones in risk assessments.

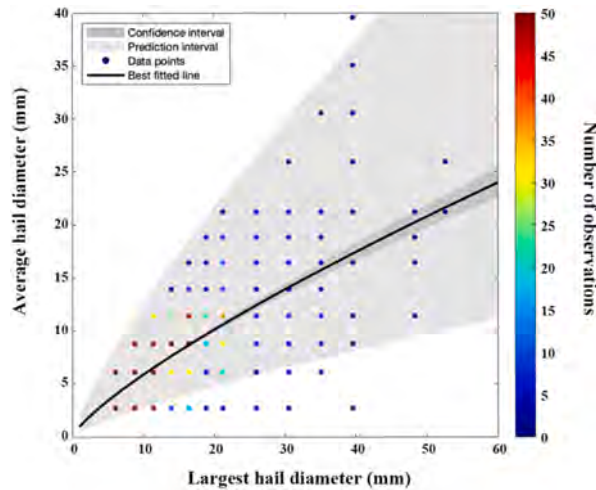


Fig. 7. Plot of  $D_a$  statistical relationship with uncertainty. The  $D_a$  data points are shown in color (most points concentrate near the center), with the best fitted line depicted in black (Equation (8)). The dark grey area represents the 95 % confidence interval for the mean prediction of  $D_a$  given  $D_l$ . The light grey represents the 95 % prediction interval for the  $D_a$  prediction given  $D_l$ . The observed data align well within the prediction interval, indicating a consistent statistical relationship fit.

2.3. Relationship between  $D_l$  and hailstorm duration

Fig. 8a and b shows the histogram of duration, and the number of observations of duration on each  $D_l$ . The average duration is plotted in Fig. 8c. The duration variance increases as  $D_l$  increases, because there are more hail cases under small  $D_l$  than large  $D_l$ . The hailstorm duration, denoted by  $T$  (in minutes), is assumed to have a relationship with  $D_l$  in a power function [22]

$$\log_{10} T = \log_{10} a_T + b_T \log_{10} D_l + \epsilon_T, \tag{9}$$

where  $a_T = 4.6316$ , with 95 % confidence interval (3.493, 6.142),  $b_T = 0.3167$ , with 95 % confidence interval (0.226, 0.4074) in this study, and an error term  $\epsilon_T \sim Normal(0, 0.0014)$ . Fig. 8d shows that the duration statistical relationship is similar to the previous study by Ref. [22]. The black and blue lines represent the statistical relationship fitted by Ref. [22] and this study, respectively.

In Fig. 9, the data points alongside the large prediction interval indicates considerable variability and uncertainty in hailstorm duration and their correlation to hailstone size. This uncertainty in duration significantly affects subsequent predictions of hit rates and the number of hailstones per hailstorm event, as described by Equation (10). Therefore, quantifying the uncertainty is crucial, which will be shown in later sections.

2.4. Relationship between  $D_l$  and hit rate

Fig. 10a and b shows the histogram of hit rate and the number of observations of hit rate on each  $D_l$ . The average hit rate is plotted in Fig. 10c. The hit rate ( $Hr$  in  $m^{-2}s^{-1}$ ) is calculated as

$$Hr = \frac{N_{stone}}{T \times 60 \times 0.0929}, \tag{10}$$

where  $N_{stone}$  is the number of hailstones on hailpad (the hailpad area equals  $0.0929 m^2$ ) and  $T$  is the hailstorm duration in minutes. As suggested by Ref. [22],  $Hr$  can be estimated by  $D_l$  as a power function

$$\log_{10} Hr = \log_{10} a_{Hr} + b_{Hr} \log_{10} D_l + \epsilon_{Hr}, \tag{11}$$

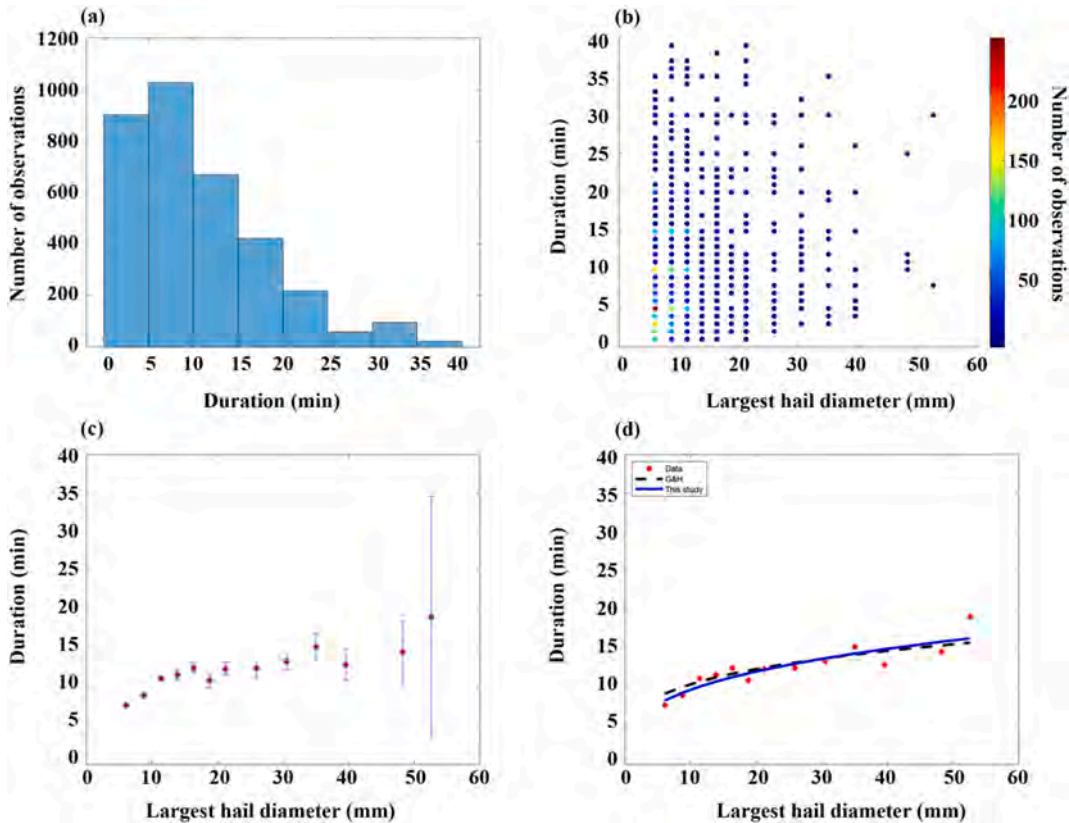


Fig. 8. Duration plots. (a) Histogram of duration. (b) The scatter plot of duration under each unique  $D_l$ , with color indicating the number of observations. (c) Averaged duration plot with variation bar. (d) Duration statistical relationship comparison plot.

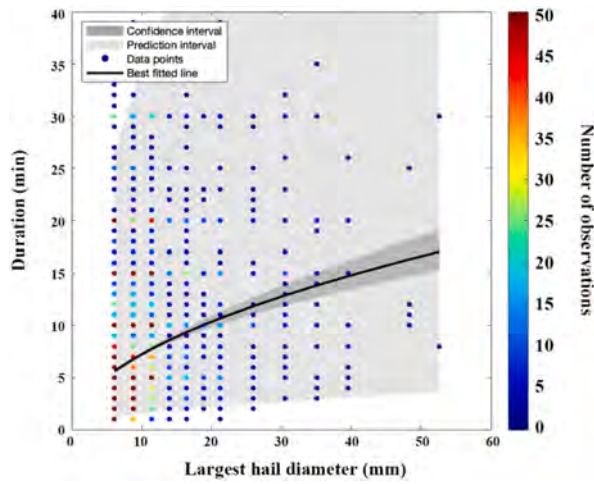


Fig. 9. Plot of duration statistical relationship with uncertainty. The duration data points are shown in blue, with the best fitted line depicted in black (Equation (9)). The dark grey area represents the 95 % confidence interval for the mean prediction of the duration given  $D_i$ . The light grey represents the 95 % prediction interval for the duration prediction given  $D_i$ .

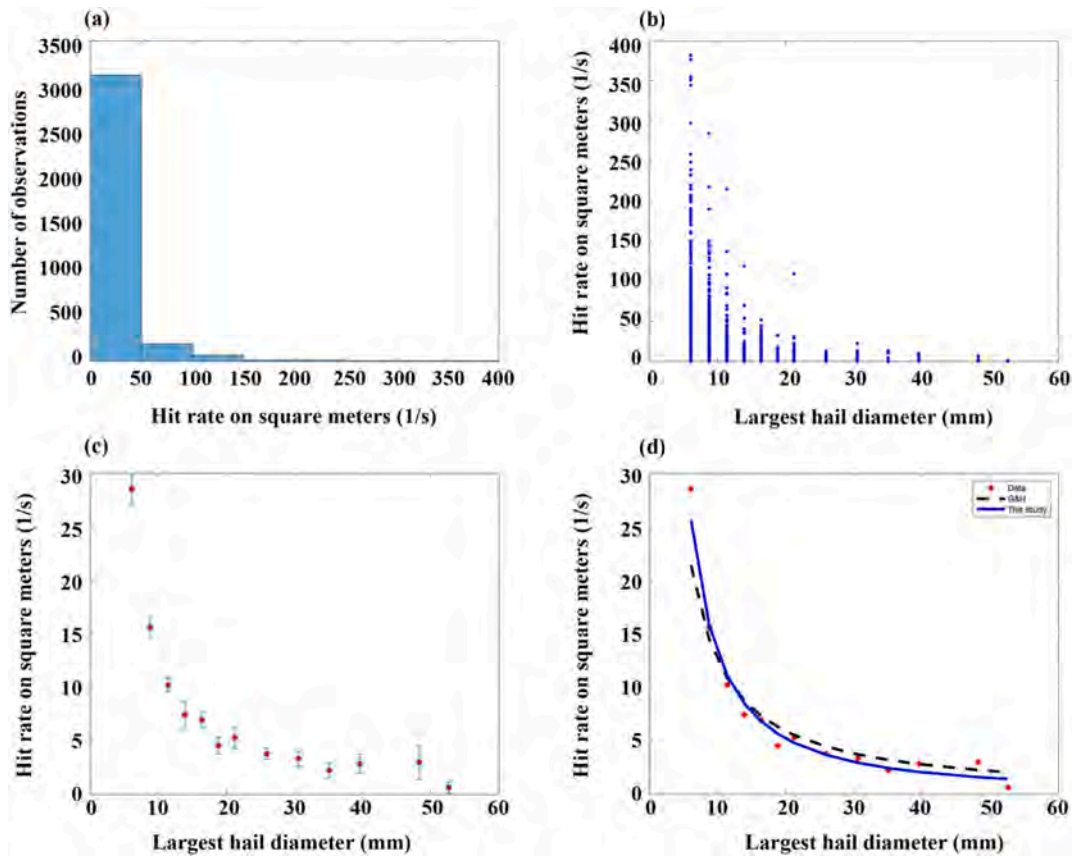


Fig. 10. Hit rate plots. (a) Histogram of hit rate. (b) The scatter plot of hit rate under each unique  $D_i$ , with color indicating the number of observations. (c) Average hit rate plot with variation bar. (d) Hit rate statistical relationship comparison plot.

where  $a_{Hr} = 294$ , with 95 % confidence interval (108, 802),  $b_{Hr} = -1.345$  with 95 % confidence interval ( - 1.668, - 1.022), and an error term  $\epsilon_{Hr} \sim Normal(0, 0.0181)$ . Fig. 10d shows that the hit rate statistical relationship is similar to Ref. [22]. The black and blue lines represent the statistical relationship fitted by Ref. [22] and this study, respectively.

Fig. 11 shows a decreasing trend of the hit rate of hailstones with increasing hail diameter, accompanied by a notable degree of uncertainty as depicted by the spread of data points and the substantial width of the prediction interval. This uncertainty underscores

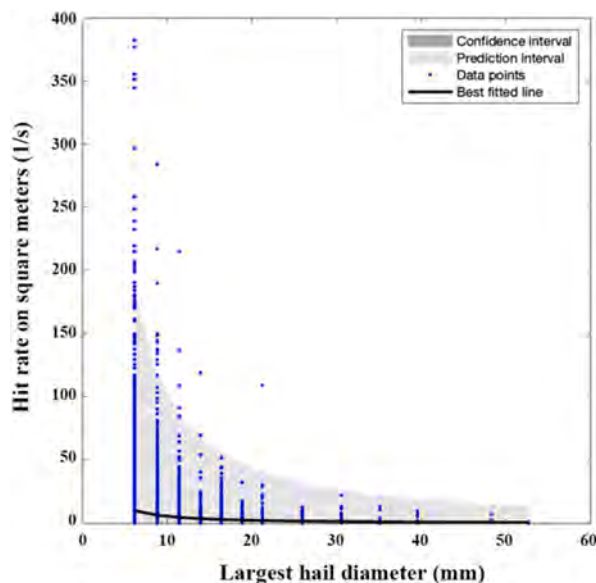


Fig. 11. Plot of hit rate statistical relationship with uncertainty. The hit rate data points are shown in blue, with the best fitted line depicted in black (Equation (11)). The dark grey area represents the 95 % confidence interval for the mean prediction of the hit rate given  $D_l$ . The light grey represents the 95 % prediction interval for the hit rate prediction given  $D_l$ .

the challenges of predicting hailstone impact frequencies. Accounting for this variability is crucial in creating an accurate model for hailstorm characterization and risk assessment.

### 3. Methodology for hail roof damage calculation and uncertainty analysis

The method for estimating the probability of hail damage on roofs during a hailstorm utilizes the approach outlined by Ref. [24]. This method calculates the probability of roof failure due to each hailstone impact during a hailstorm. Uncertainty in this calculation is addressed in model prediction uncertainty, which pertains to the variability of the parameters (coefficients and normal error term). The subsequent two subsections elaborate the specifics of uncertainty analysis and the hail risk assessment.

#### 3.1. Uncertainty analysis on model prediction

In Section 2, hail statistical relationships are developed to characterize the distribution of the largest hail diameter  $D_b$ ,  $D_a$ , the duration of hailstorms, and the hit rate of hailstones. These statistical relationships are shown in Figs. 5, 7, 9 and 11, where broad prediction intervals indicate substantial uncertainty in the variable prediction of the hail statistical relationships. The width of these intervals suggests that while the statistical relationship can capture general trends, there is a significant range within which the actual values could fall, reflecting the nature of hail phenomena and the inherent challenges in precisely predicting such variable environmental conditions. The notable uncertainty in the hail hazard model highlights the need to refine the model by considering the range of the prediction interval. By employing Monte Carlo simulations, statistical relationships are fitted accounting the uncertainty to capture a range of possible outcomes. For example, a value of  $D_l$  is first simulated from the probability distribution estimated in Equation (5). Then,  $\log(D_a)$  is estimated by summing the average  $\log(D_a)$  estimated by the given  $D_l$  (Equation (8)) and a random scaling factor (following  $Normal(0,1)$ ) times its standard deviation, which can be obtained from the  $D_a$  statistical relationship. The same calculation applies to the duration and hit rate. The simulated values are shown in Fig. 12. This process will update the estimations of hail characteristics and yield revised calculations of the roof damage. Through this iterative process, the model captures a realistic range with uncertainty.

#### 3.2. Method of calculating hail roof damage

A fragility function quantifies the relationship between the probability of an undesirable event and an environmental force. This study calculates the probability of exceedance for a specific limit state of a roof shingle caused by hailstones, such as tears, fractures, cracks, splits, ruptures, and any other signs of openings through the cross section of the roof, based on the diameter of the hailstones causing the impact [24]. applied fragility methods [35] to construct parametric probability distributions as fragility functions for different roof types, including a baseline non-impact-resistant roof and four graded impact-resistant options. The non-impact-resistant roof serves as a baseline for comparison. Impact-resistant roofs are classified in an increasing order, with Class 1 roofs withstanding single impact of a 1.25-inch ice sphere, Class 2 roofs withstanding single impact of a 1.5-inch ice sphere, Class 3 roofs withstanding single impact of a 1.75-inch ice sphere, and Class 4 roofs withstanding single impact of a 2.0-inch ice sphere. These classifications are based on the absence of shingle cracking or breaking when subjected to steel (UL 2218 Standard) and ice (FM 4417 Standard) balls dropped from heights designed to simulate the kinetic energy of terminal velocity hailstone impacts [36,37]. The source of data for

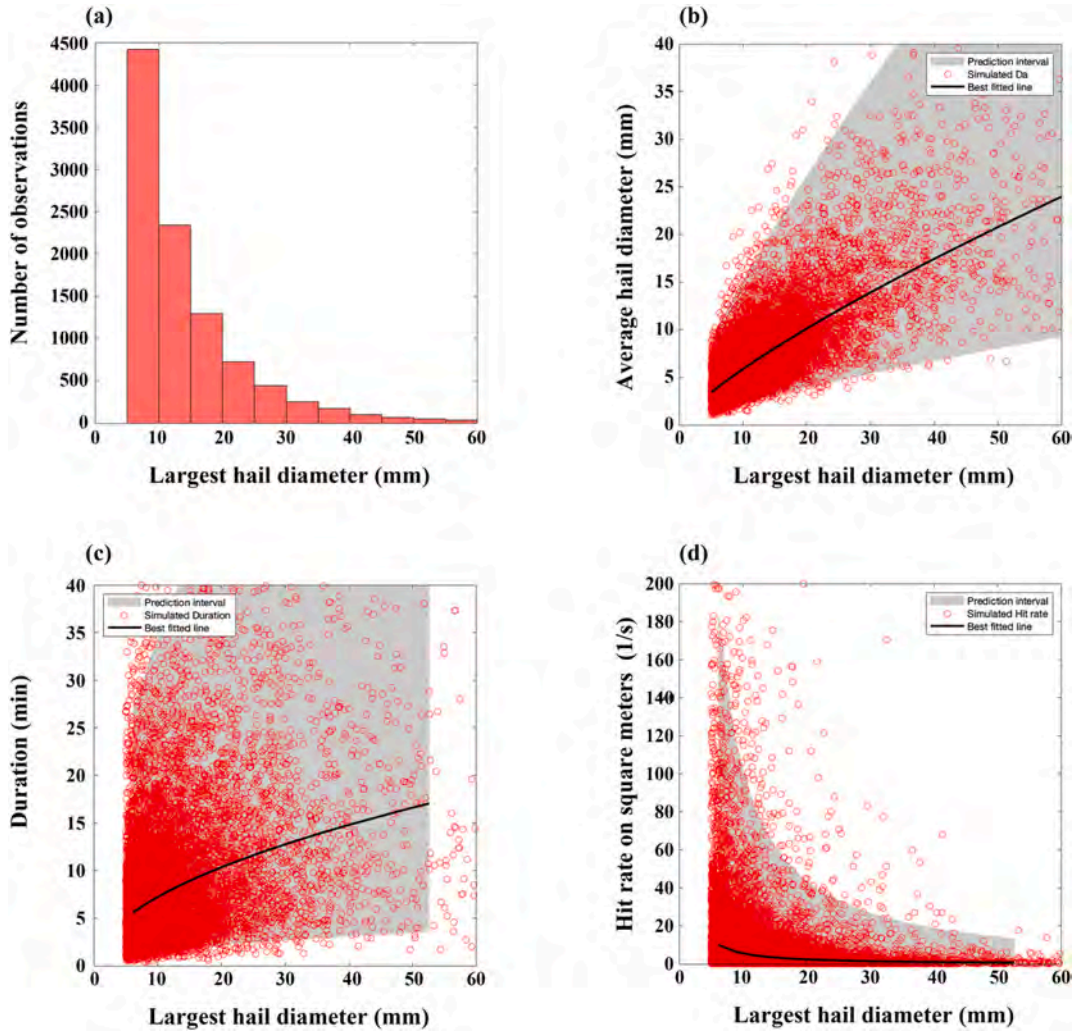


Fig. 12. Simulated values for  $D_b$ ,  $D_a$ , duration, and hit rate. They match with their prediction intervals.

these fragility functions comes from experimental tests previously done by Ref. [38], which involved using ice balls made from tap water to mimic hailstones [24] The experiments measure the shingles resistance to different ice ball sizes. The results are used to fit lognormal cumulative distribution functions, quantifying the probability of failure. The fragility function is expressed as

$$P_f(x) = \Phi\left(\frac{\ln\left(\frac{x}{\theta}\right)}{\gamma}\right), \tag{12}$$

where  $P_f(x)$  denotes the probability of failure of a roof,  $x$  is the hailstone diameter,  $\Phi(\bullet)$  denotes the standard normal cumulative distribution function,  $\theta$  and  $\gamma$  are parameters of the distribution, which denotes the median capacity and measures variability in capacity, respectively. Fig. 13 summarizes the overall risk calculation for this process.

To apply the fragility function, first determine the number and size of hailstones impacting a shingle. Then, using the statistical relationships from Section 2, derive the  $D_a$  for Gamma parameters, and duration ( $T$ ) and hit rate ( $Hr$ ) for the total count of hailstones ( $N$ ). Following this, the diameter distribution function  $F_D(d)$  allows for the estimation of the number of hailstones having certain hailstone sizes. The probability of a roof shingle damage in a hailstorm whose maximum hail diameter is given is [24]

$$P_{fail}(D_l) = 1 - \prod_{x=3}^{D_l} \left(1 - \Phi\left(\frac{\ln\left(\frac{x}{\theta}\right)}{\gamma}\right)\right)^{N_{ab}}, \tag{13}$$

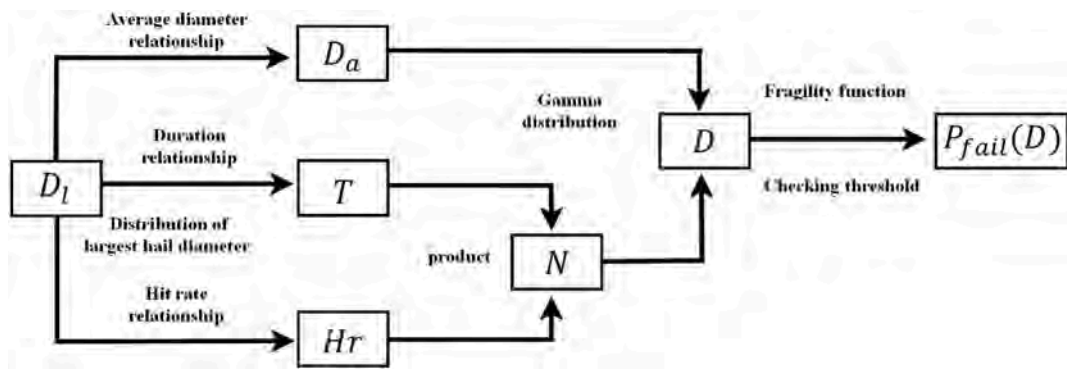


Fig. 13. Flow chart of hail risk calculation.

where  $x = \hat{I} \{5, 6, 7, \dots, D_l\}$ ,  $a = x - 0.5$ , and  $b = x + 0.5$ .  $N_{ab}$  is the number of hailstone observations whose diameters are between  $a$  and  $b$  mm on one shingle, calculated as

$$N_{ab} = N \times A \times f_{ab}, \tag{14}$$

where  $N$  is the total number of hailstone observations per unit area calculated by  $T$  and  $Hr$ ,  $A$  is the exposed area of a shingle and is taken to be  $0.165\text{m}^2$ , and  $f_{ab}$  is the probability of having a hailstone whose diameter is between  $a$  and  $b$  mm, and can be calculated as

$$f_{ab} = F_D(b) - F_D(a). \tag{15}$$

The fragility curves of the roofs provided by Ref. [24] are plotted in Fig. 14, and their parameters  $\theta$  and  $\beta$  are listed in Table 2. Fig. 14 illustrates that the higher class of the roof is associated with the lower failure probability.

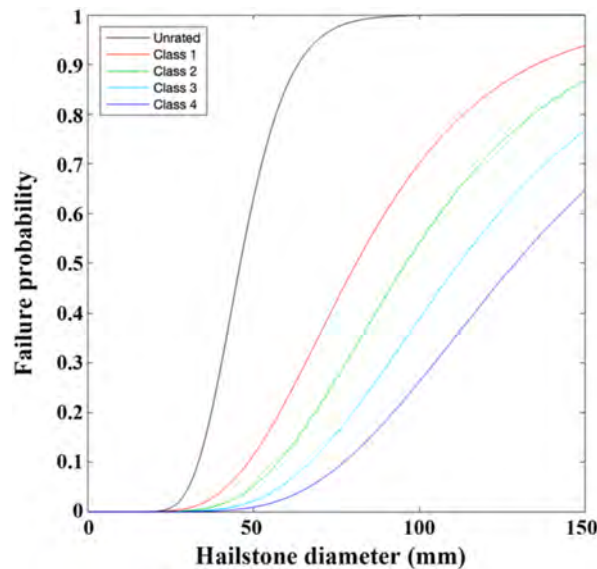


Fig. 14. Fragility curves for each hailstone during a hail event. The black, red, green, light blue, and dark blue curves represent unrated, Class1, Class 2, Class 3, and Class 4, respectively.

Table 2  
Shingle fragility parameter for roof failure by each hailstone during a hail event.

Roof type	$\theta$ (mm)	$\gamma$
Unrated	46	0.25
Class 1	81	0.4
Class 2	96	0.4
Class 3	112	0.4
Class 4	129	0.4

Many studies have explored the damage by hail and ice impact [38–40]. Two methods are employed to fit fragility curves, one tailored for unrated roofs and another for impact-resistant roofs [35]. For detailed information on the methodologies used to fit these curves, refer to Refs. [24,35]. Here is a concise overview of the fragility curves [24], implemented experimental specimens [38] using ice balls to strike shingles, calculating the failure rate of each roof type in relation to the diameter of the ice balls used. For the unrated roof, the fragility curve is fitted by “bounding diameter” (Method B in Ref. [35]), where it is known that some shingles fail under specific diameter to which they are subjected. The specimens are categorized into groups based on ranges of diameter, where each bin has about the same number of specimens. Then, calculating the proportion of specimens that fail within each range and the average diameter for each bin. These serve as independent data points representing failure probability and the diameter observed. Subsequently, these data points are transformed into an inverse cumulative distribution to construct the fragility curve. For impact-resistant roofs, the fragility curve is determined using the “capable diameter” approach (Method C in Ref. [35]), where the specimen diameter is known but no specimen fails. Impact-resistant roofs exhibit high durability, which making failure cases rare. In this analysis, the largest diameter in the dataset (denoted by  $r_{max}$ ) is assigned a low failure probability (denoted by  $F$ ). These values are sufficient to establish the cumulative distribution function [24].

The term  $P_{fail}(D_l)$  with

$$P_{fail}(D_l) = \begin{cases} P_{fail}(D_l), & P_{fail}(D_l) < E \\ 1, & P_{fail}(D_l) \geq E \end{cases}, \tag{16}$$

represents the expected proportion of a roof that would need replacement, assuming only the damaged section is repaired. A critical threshold is set at  $E = 0.5$ . If  $P_{fail}(D_l)$  exceeds this value, it will be rounded up to 1, indicating that a replacement of the entire roof is warranted when the damage exceeds half of the roof's area (Equation (16)).

#### 4. Hail risk results

##### 4.1. Hail risk analysis without uncertainty

Without uncertainty means that the mean values of hail information across each  $D_l$  are used for statistical relationship fitting. For example, the duration in Fig. 8b spread across each  $D_b$ , their mean value is computed in the modeling process, as demonstrated in Fig. 8c. The averaged data provide a general indication of trends, serving as a basic framework for estimating hail hazards and risks. In accordance with the methods outlined in Section 3.2, this study calculates the average proportion of the probability of hail damage on roofs. By simulating 10,000 hail events that produce  $D_l = 5$  mm or greater, the study calculates the mean probability of hail damage on roofs, which is summarized in Table 3.

Table 3 presents the risk outcomes from the analysis conducted without considering hail hazard uncertainty, under three different values of  $\alpha$ . It is observed that a larger  $\alpha$  corresponds to a smaller probability of extensive damage. According to Ref. [32], the longer delay in sampling data leads to smaller  $\alpha$ , implying that a smaller  $\alpha$  reflects a larger original hail diameter due to increasing melting time. Figs. 15 and 16 show the distributions of the hail risk output and the cases of whole roof replacement. A consistent finding across these figures is that a smaller  $\alpha$  results in more extensive roof replacements. For comparative analysis of roof types, this study selects the scenario where  $\alpha$  equals to 1.75 for simplicity. An unrated roof typically incurs approximately 5.4 % damage, whereas roofs with impact resistance classifications exhibit considerably less damage, ranging from 2.3 % for the least resistant class to as low as 0.11 % for the highest resistance class as shown in Table 3. This represents a substantial reduction in the probability of hail damage, from about 60 % to as much as 98 %, when compared to the unrated roof as a baseline. Fig. 16 corroborates these results, showing that higher class roofs predominantly suffer minimal whole roof replacement (i.e.,  $P_{fail}(D_l) > 0.5$ ), with over 400 cases in unrated roof while none are observed in Class 4 (for the simulation runs of 10,000).

##### 4.2. Hail risk analysis with uncertainty

Utilizing the methodology specified in Section 3, this section computes the hail roof damage by factoring in the model's variable prediction uncertainty (Figs. 5, 7, 9, 11 and 12). The analysis conducted total 10,000 hypothetical hailstorms and calculated 10,000 independent probability of hail damage. In individual simulations, the variables were estimated within the predictive range that incorporates the inherent uncertainty within the prediction intervals for  $D_b$ ,  $D_a$ ,  $T$ , and  $Hr$  statistical relationships.

Table 4 presents the roof damage outcomes from the analysis conducted with considering hail hazard uncertainty, under three different values of  $\alpha$ . It is observed that a larger  $\alpha$  corresponds to a smaller probability of extensive damage (same as the previous results). Figs. 17 and 18 show the distributions of the risk output and the cases of whole roof replacement. A consistent finding across these figures is that a smaller  $\alpha$  results in more extensive roof replacements. For comparative analysis of roof types, this study selects the scenario where  $\alpha$  equals to 1.75 for simplicity. An unrated roof typically incurs approximately 7.6 % damage,

**Table 3**  
Summary of the probability of hail damage on roofs without uncertainty analysis on hail hazard.

Gamma parameter	Unrated	Class 1	Class 2	Class 3	Class 4
$\alpha = 1.5$	0.0566	0.0236	0.0093	0.0032	0.0011
$\alpha = 1.75$	0.0539	0.0228	0.0091	0.0031	0.0011
$\alpha = 2.0$	0.0535	0.0224	0.0089	0.0030	0.0010

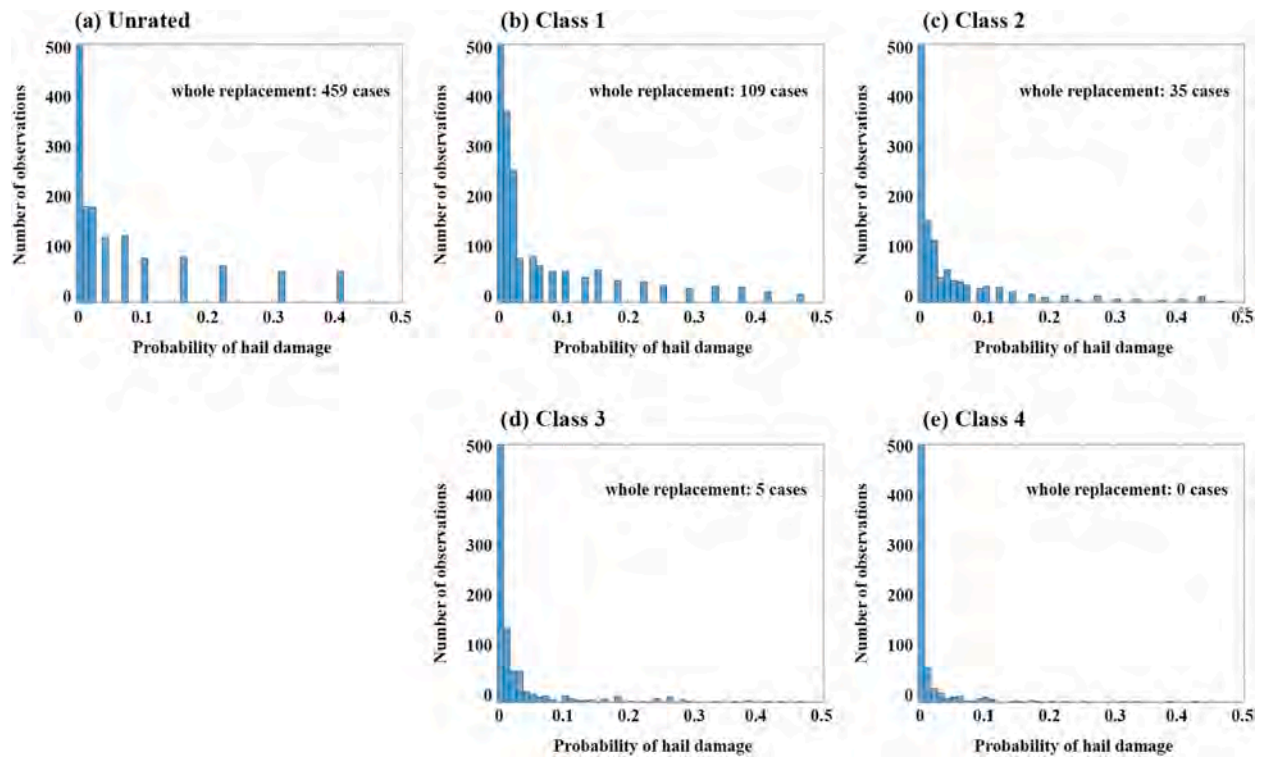


Fig. 15. The distribution of the probability of hail damage without uncertainty analysis under  $\alpha = 1.5$ .

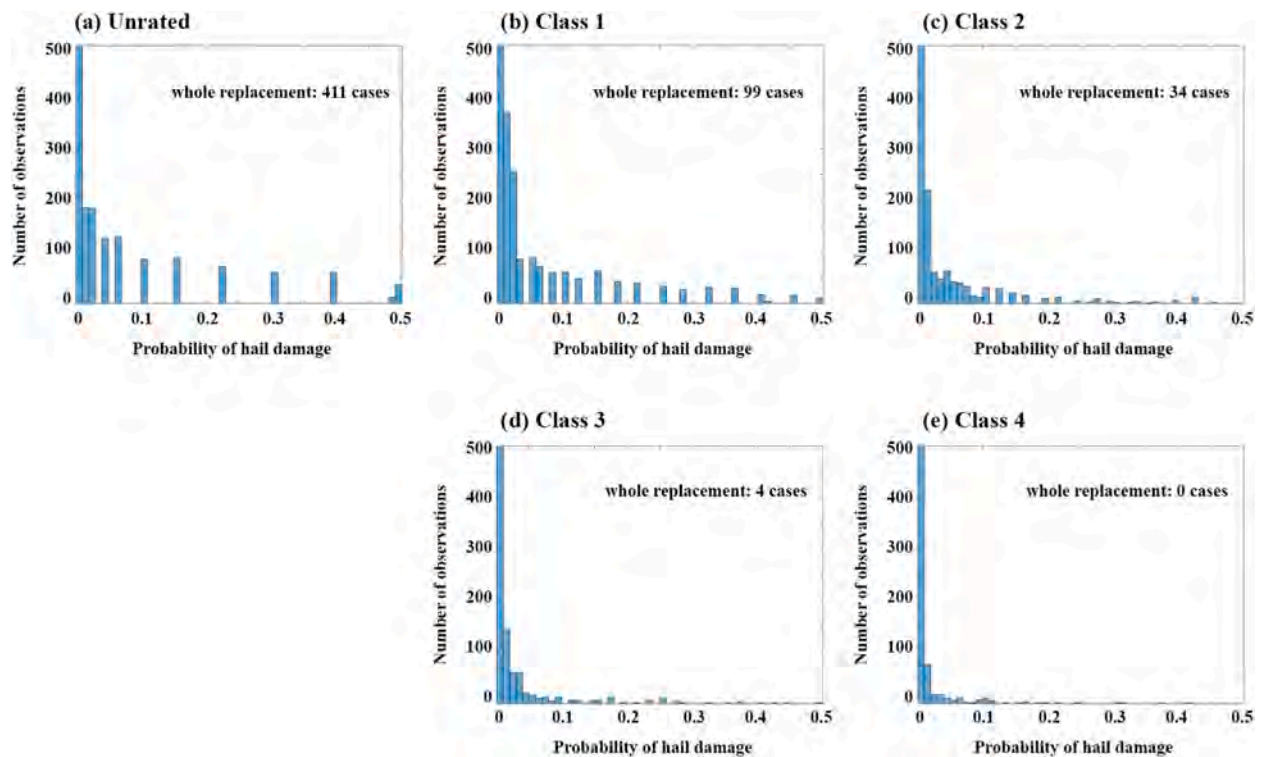


Fig. 16. The distribution of the probability of hail damage without uncertainty analysis under  $\alpha = 1.75$ .

**Table 4**  
Summary of the probability of hail damage on roofs with uncertainty analysis on hail hazard.

Gamma parameter	Unrated	Class 1	Class 2	Class 3	Class 4
$\alpha = 1.5$	0.0767	0.0448	0.0264	0.0159	0.0096
$\alpha = 1.75$	0.0755	0.0441	0.0259	0.0155	0.0094
$\alpha = 2.0$	0.0741	0.0436	0.0254	0.0150	0.0092

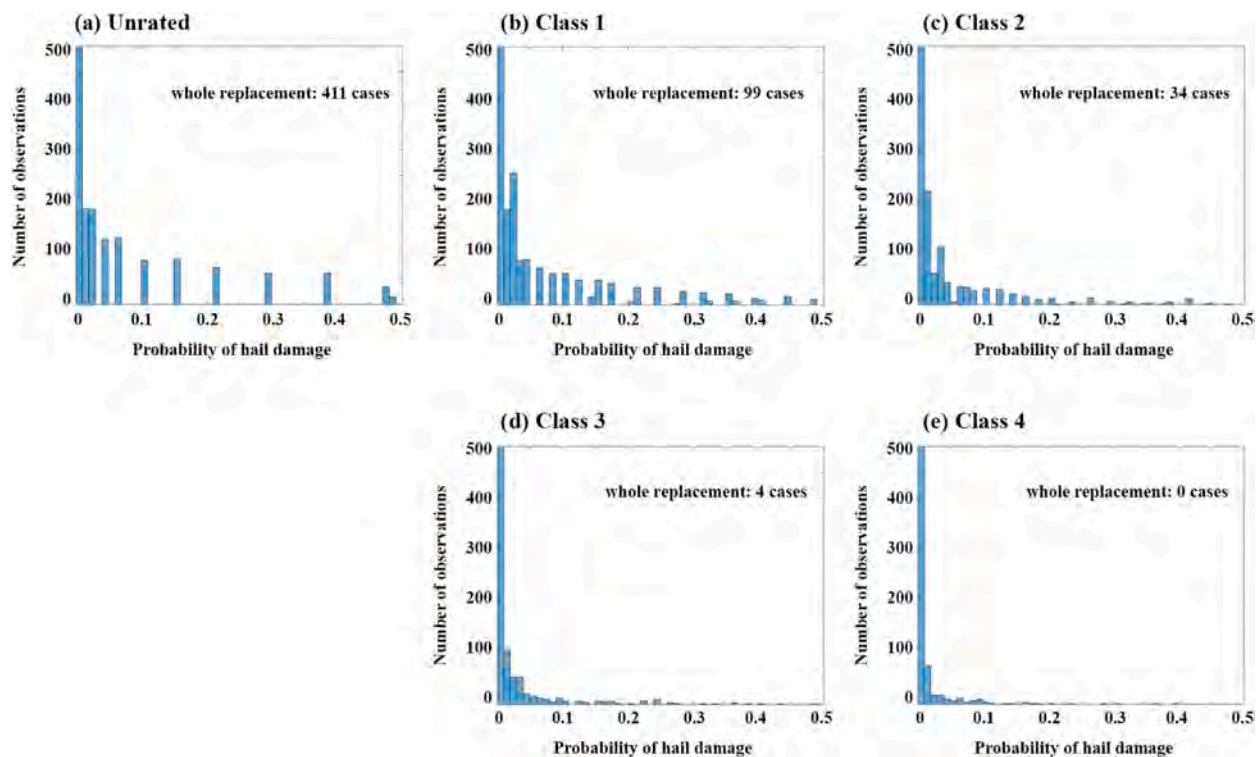


Fig. 17. The distribution of the probability of hail damage without uncertainty analysis under  $\alpha = 2.0$ .

whereas roofs with impact resistance classifications exhibit considerably less damage, ranging from 4.4 % for the least resistant class to as low as 0.94 % for the highest resistance class as shown in Table 4. This represents a substantial reduction in the probability of hail damage, from about 40 % to as much as 90 %, when compared to the baseline case of unrated roof (Figs. 19 and 20).

To examine the impact of hail hazard uncertainty, the outcome of  $\alpha = 1.75$  in both Tables 3 and 4 can be compared. For unrated roof, the probability of hail damage increases from 5.4 % to 7.6 %, marking a 40 % rise. Regarding the impact-resistance roofs, an averaged increment of 460 % of probability of hail damage, with 190 %, 290 %, 500 %, and 850 % for Class1 through 4, respectively. The significant increase in the probability of hail damage for higher-end roof classes can be attributed to more extreme hailstorms that are likely to produce larger hailstones are simulated, and they can damage even the resistant roofs. Figs. 18–20 corroborate this conclusion, showing that the number of cases of whole replacement is higher than the number of cases indicated in Figs. 15–17. The increase of cases is especially evident for Class 3 and 4, from 4 to 0 to 102 and 64 cases, respectively, when hail hazard uncertainty is incorporated into the modeling. Fig. 21 shows that incorporating uncertainty into the hail hazard model increases the exceedance probability, which could indicate a more conservative estimate of risk. In the figure, semi-logarithmic scale is used to show the effect of the uncertainty in the hail hazard model.

Fig. 22 illustrates the impact of individual variables to check which variable in the hail hazard model exerts the most influence when uncertainty is accounted for. Four varied models ( $\alpha = 1.75$ ) consider the uncertainty of only one specific hail hazard variable at a time during model fitting. For example, the blue line in Fig. 22 represents the scenario where only  $D_l$  uncertainty is considered, while the other variables are assumed to be certain. The black line shows the probability of hail damage for the five roof types (as discussed in Section 4.1) without uncertainty, and it is close to the uncertainty statistical relationships of  $D_a$ ,  $T$ , and  $Hr$ . This analysis suggests that the inclusion of uncertainties in  $D_a$ ,  $T$ , and  $Hr$  does not significantly alter the hail damage on roofs. However, the model that incorporates  $D_l$  uncertainty shows a higher probability of hail damage compared to the others, indicating that  $D_l$  uncertainty has the most significant impact on roof damage calculations.

Table 5 highlights the number of roof replacement cases across different roof types under varying conditions of uncertainty within the hail hazard model, indicating substantial differences in the impact of each type of uncertainty on decision-making. Notably, the inclusion of  $D_l$  uncertainty leads to a significant increase in roof replacements for all classes, underscoring the critical in-

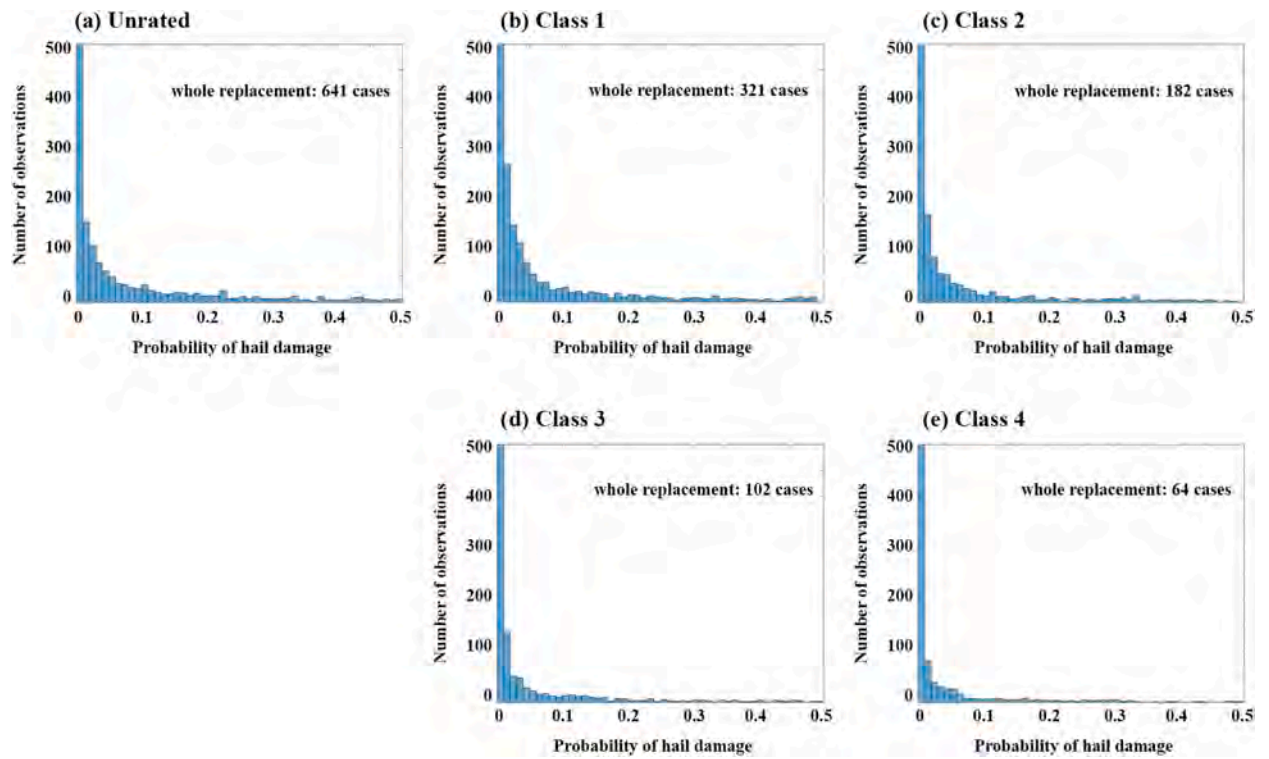


Fig. 18. The distribution of the probability of hail damage with uncertainty analysis under  $\alpha = 1.5$ .

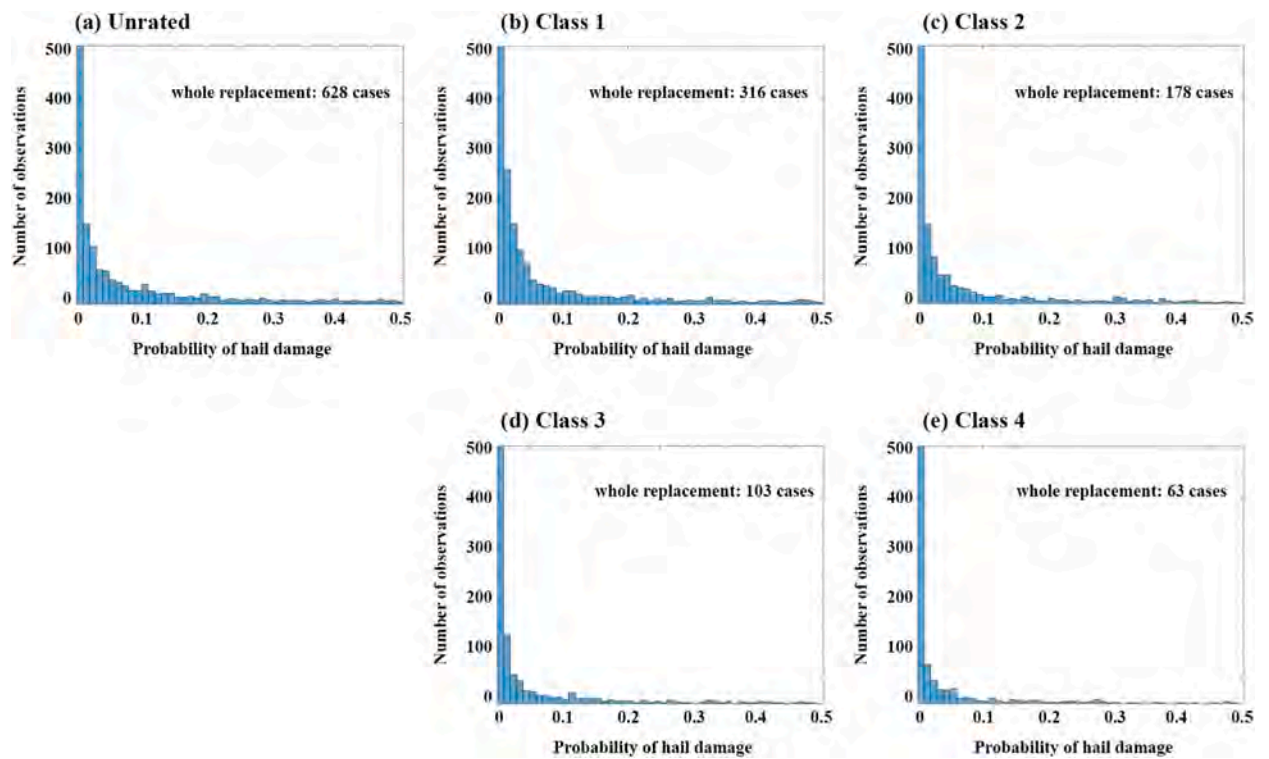


Fig. 19. The distribution of the probability of hail damage with uncertainty analysis under  $\alpha = 1.75$ .

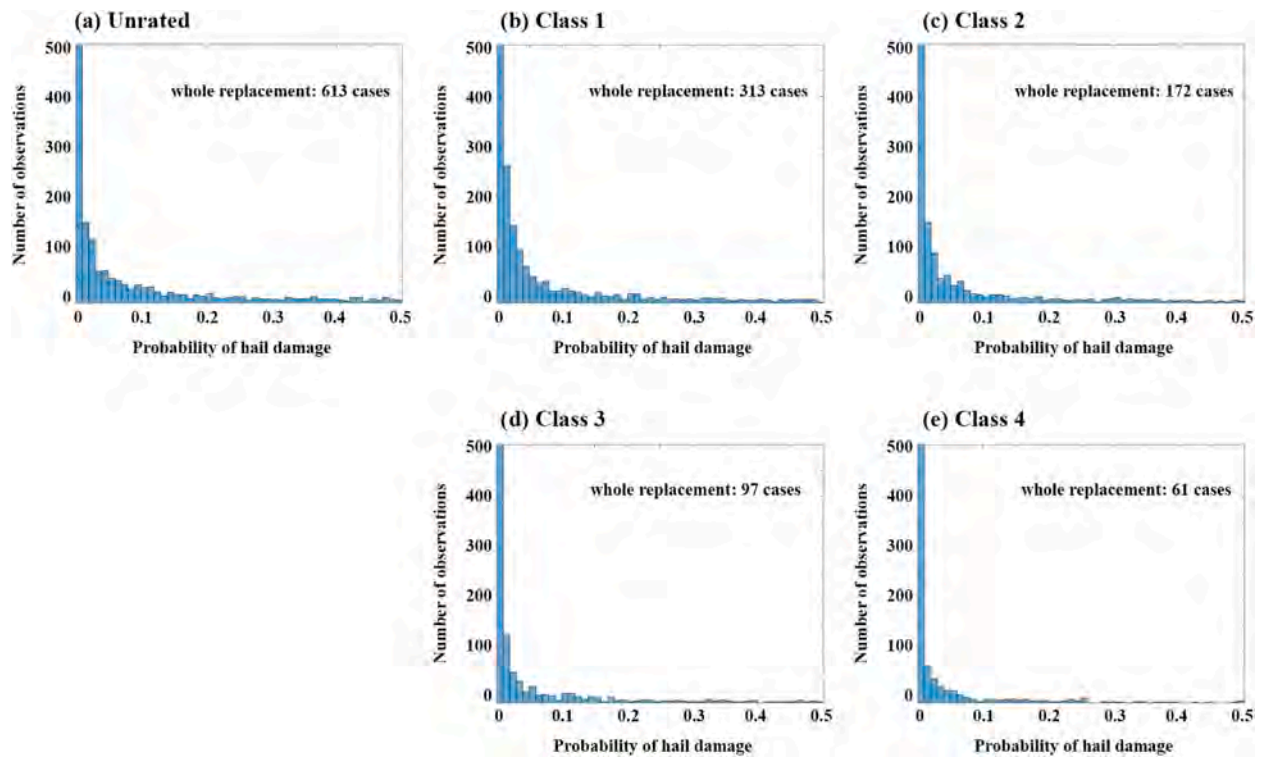


Fig. 20. The distribution of the probability of hail damage with uncertainty analysis under  $\alpha = 2.0$ .

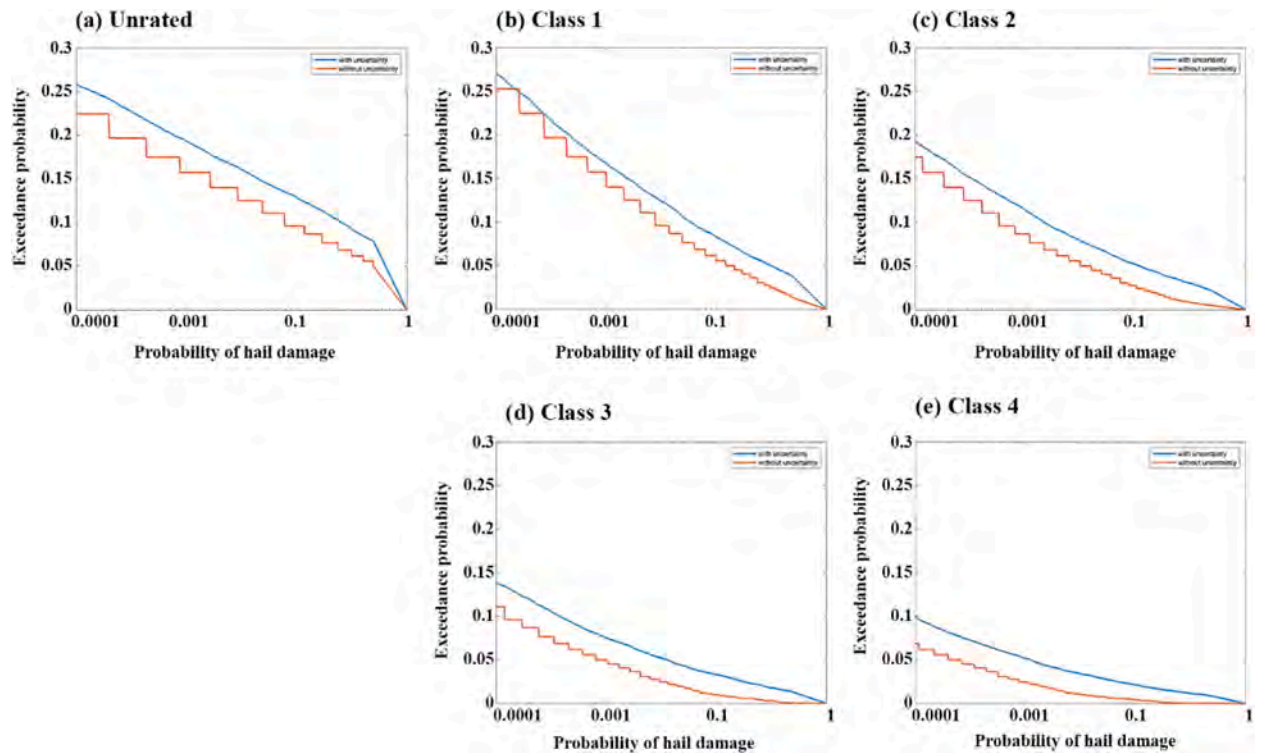


Fig. 21. The log-based comparison for exceedance probability of hail damage with and without uncertainty under  $\alpha = 1.75$ . The exceedance probability indicates the likelihood of probability of hail damage exceeding a certain threshold.

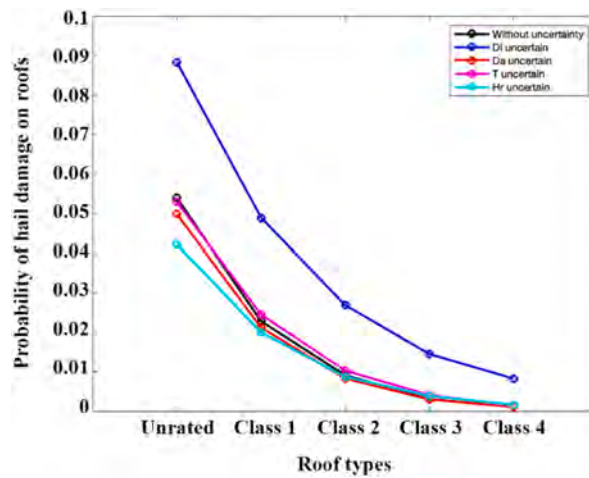


Fig. 22. Comparison of the probability of hail damage under individual hail hazard variable uncertainty models.

Table 5

Whole replacement cases under individual hail hazard variable uncertainty models (out of 10,000 simulation runs).

	Unrated	Class 1	Class 2	Class 3	Class 4
Without uncertainty	411	99	34	4	0
$D_l$ uncertain	720	317	173	81	46
$D_a$ uncertain	381	99	30	6	2
$T$ uncertain	411	127	46	14	2
$H_r$ uncertain	309	109	44	18	5

fluence that  $D_l$  exerts in estimating the hail damage. In comparison, although uncertainties in  $D_a$ ,  $T$ , and  $H_r$  lead to relatively smaller changes in replacement cases, the number of whole roof replacement cases increases compared with model without uncertainty. This suggests that while  $D_a$ ,  $T$ , and  $H_r$  impact is less pronounced than  $D_l$ , these factors contribute to some extreme hailstorm that can deal damage to high classed roofs.

### 5. Conclusion and discussion

The statistical modeling approach and updated CoCoRaHS data used in this study have provided valuable insights into hail hazard characterization and hail roof damage. The findings regarding the resistance of rated roofs for hail impact compared to unrated roofs are valuable from practical viewpoints. As the impact-resistance rating of the roof increases, the study showed improved endurance and decreased failure probability. This highlights the importance of considering the higher quality of roofs in assessing hail risk and underscores the potential benefits of investing in higher-rated roofing materials. The uncertainty analysis conducted in this study has also revealed key factors. Ignoring the uncertainty of hail hazard leads to potential underestimation of the hail risk. The uncertainty analysis serves as a critical guide for roof selection and highlights the variability and complexity inherent in hail risk assessments. It is essential for building owners and the roofing industry to consider the hail hazard uncertainty, especially improving the precise of  $D_l$  measurements or predictions to effectively manage hail risks. Additionally, insurance companies might find this analysis useful for adjusting premiums and coverage options, particularly in regions prone to hail, by acknowledging that uncertainties, especially in  $D_l$ , can significantly influence potential claims.

This study has several limitations that should be acknowledged. Firstly, it is important to note that hail damage is influenced by factors, such as the number of hailstones per unit area, hailstone size, and the accompanying winds [41]. However, due to limitations in wind data, this study only considers hailstone size, hailstorm duration, and hit rate, without accounting for the wind effect. Secondly, this study does not account for differences in hailstone impacts that occur over different geographical areas or varying conditions within a localized region. The dataset encompasses at least two different meteorological environments (CoCoRaHS is from the U.S. and the roof is from Calgary, Canada). This variation could result in different characteristics within the hail size distribution across the regions studied. Additionally, the accuracy of the fragility model is limited by the challenge of simulating real hailstone falls from the clouds. Laboratory conditions may not perfectly replicate the dynamics of natural hailstorms as well as the influence of wind and other atmospheric factors. Besides, the Gamma shape factor ( $\alpha$ ) in hailstone diameter distribution is selected arbitrarily (within a reasonable range). To address these limitations, future research could integrate additional databases with the current model and consider incorporating new data and technological advancements to enhance our understanding and improve the accuracy of predicting hail hazards and risks.

**Funding**

This study is supported by the Natural Sciences and Engineering Research Council of Canada - Alliance Grants (ALLRP 576691-22).

**CRedit authorship contribution statement**

**Yao Li:** Writing – original draft, Visualization, Validation, Methodology, Investigation, Formal analysis. **Keith Porter:** Writing – review & editing, Supervision, Methodology, Investigation, Conceptualization. **Katsuichiro Goda:** Writing – review & editing, Supervision, Project administration, Funding acquisition, Conceptualization.

**Declaration of competing interest**

The authors declare the following financial interests/personal relationships which may be considered as potential competing interests:

Yao Li reports financial support was provided by Natural Sciences and Engineering Research Council of Canada. If there are other authors, they declare that they have no known competing financial interests or personal relationships that could have appeared to influence the work reported in this paper.

**Data availability**

Data will be made available on request.

**APPENDIX**

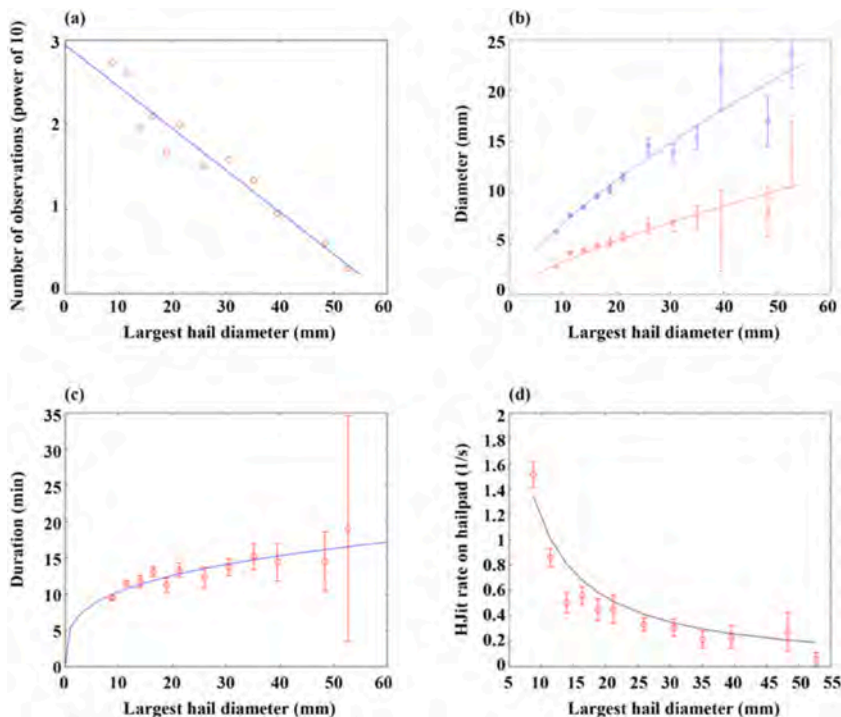


Fig. A1. Reproduction of hail relationships. (a) Largest diameter size statistical relationship. (b) Average (blue) and smallest (red) diameter statistical relationships. (c) Duration relationship. (d) Hit rate statistical relationship. Circles are sample averages, lines are best-fit function, and vertical bar are standard errors. These results are similar to Fig. 1 in Grieser and Hill (2019).

**Table A1**  
Table of the mean hail roof damage.

Roof	Porter	NHP
Unrated	0.057	0.053
Class 1	0.030	0.028

(continued on next page)

Table A1 (continued)

Roof	Porter	NHP
Class 2	0.011	0.011
Class 3	0.0047	0.0041
Class 4	0.0011	0.0009

## References

- [1] H. Pruppacher, J. Klett, Microphysics of clouds and precipitation, in: Atmospheric and Oceanographic Sciences Library, 2010, <https://doi.org/10.1007/978-0-306-48100-0>.
- [2] American Meteorological Society Hail, Glossary of Meteorology, 2012. <https://glossary.ametsoc.org/wiki/Hail>.
- [3] K. Pojorlie, S. Doering, M. Fowle, The record-breaking vivian, south Dakota, hailstorm of 23 July 2010, Journal of Operational Meteorology 1 (2) (2013) 3–18, <https://doi.org/10.15191/nwajom.2013.0102>.
- [4] J.T. Allen, M.K. Tippett, The characteristics of United States hail reports: 1955–2014, E-Journal of Severe Storms Meteorology 10 (3) (2015) 1–31, <https://doi.org/10.55599/ejssm.v10i3.60>.
- [5] H.J. Punge, M. Kunz, Hail observations and hailstorm characteristics in europe: a review, Atmos. Res. 176 (2016) 159–184 <https://doi.org/10.1016/j.atmosres.2016.02.012>, 177.
- [6] D. Etkin, Hail climatology for Canada: an update, Institute for Catastrophic Loss Reduction, 2018. <https://www.iclr.org/wp-content/uploads/2018/03/hail-climatology-for-canada-an-update.pdf>.
- [7] B. Behlendorf, A. Jadoon, S. Penta, Rivalry and recovery: the social consequences of climatic hazards in rural India, Int. J. Disaster Risk Reduc. 46 (2020) 101488, <https://doi.org/10.1016/j.ijdrr.2020.101488>.
- [8] X. Ni, A.D. Muehlbauer, J.T. Allen, Q. Zhang, J. Fan, A climatology and extreme value analysis of large hail in China, Mon. Weather Rev. 148 (4) (2020) 1431–1447, <https://doi.org/10.1175/mwr-d-19-0276.1>.
- [9] M. Simbürger, S. Dreisiebner-Lanz, M. Kernitzky, F. Pretenthaler, Climate risk management with insurance or tax-exempted provisions? An empirical case study of hail and frost risk for wine and apple production in styria, Int. J. Disaster Risk Reduc. 80 (2022) 103216, <https://doi.org/10.1016/j.ijdrr.2022.103216>.
- [10] M. Kunz, U. Blahak, J. Handwerker, M. Schmidberger, H.J. Punge, S. Mohr, E. Fluck, K.M. Bedka, The severe hailstorm in southwest Germany on 28 July 2013: characteristics, impacts and meteorological conditions, Q. J. R. Meteorol. Soc. 144 (710) (2017) 231–250, <https://doi.org/10.1002/qj.3197>.
- [11] S.J. Childs, R.S. Schumacher, An updated severe hail and tornado climatology for eastern Colorado, J. Appl. Meteorol. Climatol. 58 (10) (2019) 2273–2293, <https://doi.org/10.1175/jamc-d-19-0098.1>.
- [12] CatIQ, 2020-06-Cat-0124-Hailstorms in Alberta, strong prairie winds, <https://www.catiq.com/UserHome>, 2024.
- [13] R. Hohl, H. Schiesser, D. Aller, Hailfall: the relationship between radar-derived hail kinetic energy and hail damage to buildings, Atmos. Res. 63 (3–4) (2002) 177–207, [https://doi.org/10.1016/s0169-8095\(02\)00059-5](https://doi.org/10.1016/s0169-8095(02)00059-5).
- [14] S. Schuster, R. Blong, K.J. McAneney, Relationship between radar-derived hail kinetic energy and damage to insured buildings for severe hailstorms in eastern Australia, Atmos. Res. 81 (3) (2006) 215–235, <https://doi.org/10.1016/j.atmosres.2005.12.003>.
- [15] F. Letson, T.J. Shepherd, R. Barthelmie, S.C. Pryor, Modelling hail and convective storms with WRF for wind energy applications, J. Phys. Conf. 1452 (1) (2020) 012051, <https://doi.org/10.1088/1742-6596/1452/1/012051>.
- [16] M.A. Cecchini, A.J. Heymsfield, R. Honeyager, P.R. Field, L.A.T. Machado, M.A.F. Da Silva Dias, Revisiting the hail radar reflectivity–kinetic energy flux relation by combining T-matrix and discrete dipole approximation calculations to size distribution observations, J. Atmos. Sci. 79 (7) (2022) 1927–1940, <https://doi.org/10.1175/jas-d-20-0373.1>.
- [17] M. Kunz, M. Puskeiler, High-resolution assessment of the hail hazard over complex terrain from radar and insurance data, Meteorol. Z. 19 (5) (2010) 427–439, <https://doi.org/10.1127/0941-2948/2010/0452>.
- [18] L. Nisi, O. Martius, A. Hering, M. Kunz, U. Germann, Spatial and temporal distribution of hailstorms in the alpine region: a long-term, high resolution, radar-based analysis, Q. J. R. Meteorol. Soc. 142 (697) (2016) 1590–1604, <https://doi.org/10.1002/qj.2771>.
- [19] J.P. Brook, A. Protat, J. Soderholm, J.T. Carlin, H.A. McGowan, R.A. Warren, HailTrack—improving radar-based Hailfall estimates by modeling hail trajectories, J. Appl. Meteorol. Climatol. 60 (3) (2021) 237–254, <https://doi.org/10.1175/jamc-d-20-0087.1>.
- [20] J.R. Bell, A. Molthan, Evaluation of approaches to identifying hail damage to crop vegetation using satellite imagery, Journal of Operational Meteorology 4 (11) (2016) 142–159, <https://doi.org/10.15191/nwajom.2016.0411>.
- [21] H.J. Punge, K.M. Bedka, M. Kunz, S.D. Bang, K.F. Itterly, Characteristics of hail hazard in South Africa based on satellite detection of convective storms, Nat. Hazards Earth Syst. Sci. 23 (4) (2023) 1549–1576, <https://doi.org/10.5194/nhess-23-1549-2023>.
- [22] J. Grieser, M. Hill, How to express hail intensity—modeling the hailstone size distribution, J. Appl. Meteorol. Climatol. 58 (10) (2019) 2329–2345, <https://doi.org/10.1175/jamc-d-18-0334.1>.
- [23] J.L. Marcos, J.L. Sánchez, A. Merino, P.H. Melcón, G. Mérida, E. García-Ortega, Spatial and temporal variability of hail falls and estimation of maximum diameter from meteorological variables, Atmos. Res. 247 (2021) 105142, <https://doi.org/10.1016/j.atmosres.2020.105142>.
- [24] K.A. Porter, A benefit-cost analysis of impact-resistant asphalt shingle roofing, Institute for Catastrophic Loss Reduction (2022). <https://doi.org/10.25810/8bcmc27>.
- [25] H. Weickmann, Observational data on the formation of precipitation in cumulonimbus clouds, Thunderstorm electricity (1953) 66–138.
- [26] A.E. Carte, R.E. Kidder, Transvaal hailstones, Q. J. R. Meteorol. Soc. 92 (393) (1966) 382–391, <https://doi.org/10.1002/qj.49709239307>.
- [27] K.A. Browning, J.G. Beimers, The oblateness of large hailstones, J. Appl. Meteorol. Climatol. 6 (6) (1967) 1075–1081.
- [28] A.J. Heymsfield, M. Szakáll, A. Jost, I.M. Giammanco, R.L. Wright, A comprehensive observational study of graupel and hail terminal velocity, mass flux, and kinetic energy, J. Atmos. Sci. 75 (11) (2018) 3861–3885, <https://doi.org/10.1175/jas-d-18-0035.1>.
- [29] R. Fraile, E. García-Ortega, Fitting an exponential distribution, J. Appl. Meteorol. 44 (10) (2005) 1620–1625, <https://doi.org/10.1175/jam2271.1>.
- [30] M.V. Sioutas, T. Meaden, J.D. Webb, Hail frequency, distribution and intensity in northern Greece, Atmos. Res. 93 (1–3) (2009) 526–533, <https://doi.org/10.1016/j.atmosres.2008.09.023>.
- [31] R. Fraile, A. Castro, L. López, J.L. Sánchez, C. Palencia, The influence of melting on hailstone size distribution, Atmos. Res. 67–68 (2003) 203–213, [https://doi.org/10.1016/s0169-8095\(03\)00052-8](https://doi.org/10.1016/s0169-8095(03)00052-8).
- [32] R.K. Wong, N. Chidambaram, L. Cheng, M. English, The sampling variations of hailstone size distributions, J. Appl. Meteorol. Climatol. 27 (3) (1988) 254–260.
- [33] R.A. Schlessensner, J.D. Marwitz, W.L. Cox, Hailfall data from a fixed network for the evaluation of a hail modification experiment, J. Appl. Meteorol. 4 (1) (1965) 61–68, [https://doi.org/10.1175/1520-0450\(1965\)004](https://doi.org/10.1175/1520-0450(1965)004).
- [34] K. Liu, P. Li, Z. Wang, Statistical modeling of random hail impact, Extreme Mechanics Letters 48 (2021) 101374, <https://doi.org/10.1016/j.eml.2021.101374>.
- [35] K. Porter, R. Kennedy, R. Bachman, Creating fragility functions for performance-based earthquake engineering, Earthq. Spectra 23 (2) (2007) 471–489.
- [36] F.M. Approvals, Specification test standard for impact resistance testing of rigid roofing materials by impacting with freezer ice balls. Class Number 4473, 2005, p. 10.
- [37] Underwriters Laboratory, UL standard for safety impact resistance of prepared roof covering materials, Northbrook IL (2020) 18.
- [38] T.P. Marshall, R.F. Herzog, S.J. Morrison, S.R. Smith, Hail damage threshold sizes for common roofing materials, 21st Conference on Severe Local Storms, August 11–16, 2002, San Antonio, TX 25 (2002) 3.2. <https://ams.confex.com/ams/pdfpapers/45858.pdf>.

- [39] Z. Wang, M. Zhao, K. Liu, K. Yuan, J. He, Experimental analysis and prediction of CFRP delamination caused by ice impact, *Eng. Fract. Mech.* 273 (2022) 108757, <https://doi.org/10.1016/j.engfracmech.2022.108757>.
- [40] K. Liu, J.L. Liu, Z. Wang, A damage threshold prediction model of CFRP panel by hail impact based on delamination mechanism, *Eng. Fract. Mech.* 239 (2020) 107282, <https://doi.org/10.1016/j.engfracmech.2020.107282>.
- [41] S.A. Changnon, D. Changnon, S.D. Hilberg, Hailstorms across the nation: an atlas about hail and its damages, ISWS Contract Report (2009). <https://experts.illinois.edu/en/publications/hailstorms-across-the-nation-an-atlas-about-hail-and-its-damages>.